ChemComm

COMMUNICATION

View Article Online
View Journal | View Issue

Cite this: *Chem. Commun.*, 2022, **58**, 10237

Received 31st May 2022,
Accepted 12th August 2022

DOI: 10.1039/d2cc03081k

rsc.li/chemcomm

Chiral gold(III) complexes: speciation, *in vitro*, and *in vivo* anticancer profile†

Adedamola S. Arojojoye,[a] Jong H. Kim,[a] Chibuzor Olelewe,[a] Sean Parkin[a] and Samuel G. Awuah*[abc]

Emerging synthetic development of chiral gold(III) complexes has prompted new opportunities in catalysis and material science with limited utility in biomedicine. Here, we demonstrate potential chemotherapeutic capability of [C^N]Au(III)Cl(R-DuPhos) (1–7) complexes, containing 1,2-bis[(2*R*,5*R*)-2,5-dialkylphospholano]benzene, which shows good stabilty, potent anticancer activity, and tolerability in mice.

Pharmacological impact of metal-based drugs including platinum and gold therapy in the clinic has been transformative in the field of cancer and rheumatoid arthritis.[1,2] Despite the clinical success, drawbacks including adverse side effects and resistance has prompted the discovery of new metallodrugs to treat different disease indications including cancer.[2,3] The use of Au(III) complexes has garnered attention due to its biocompatibility, cytotoxicity, isoelectronic character to Pt(II), and variable coordination sites.[4–6] However, the solution and physiological stability of Au(III) remains a bottleneck for chemotherapeutic development. Thus, new Au(III) structural scaffolds with improved stability to circumvent premature deactivation can bridge this gap. The synthesis of chiral Au(III) complexes is an exciting area of research with significant contributions to asymmetric catalysis and material science.[7–9] Applications of chiral Au(III) complexes as anticancer agents is underexplored but possess tremendous potential.[10] Reports using chiral diamine chelates or isothiourea ligand coordinated to $AuCl_3$ show minimal to no cytotoxicity.[11,12] To date, two reports of a diastereomeric mixture of the same chiral diphosphane chelate to a gold center is characterized as a cytotoxic chiral Au(III) complex with no evidence in support of their speciation.[6,13]

Recent work demonstrate organogold(III) complexes bearing phosphine ligands as modulators of mitochondria action in tumor cells.[14] Since the discovery of the FDA approved gold(I) anti-arthritis drug and currently repurposed for several cancer indications, much efforts have been dedicated to the synthesis of gold-phosphine complexes.

In this work, we used chiral 1,2-bis[(2*R*,5*R*)-2,5-dialkylphospholano] benzene (R-DuPhos) and arylpyridine Au(III) Cl_2 for the preparation of seven (7) cationic organometallic Au(III) chlorido complexes [cyclometallated arylpyridine-Au(III)Cl (R-DuPhos)] (**1**–**7**; Fig. 1). Carbon stabilizing Au(III) chlorido complexes supported by chiral P^P-ligands are uncommon. With regards to R-DuPhos, it has been deployed as ancillary ligands for various transition metal complexes such as Pt, Pd, Ir, Rh. Much of their application is in asymmetric catalysis with Pt-DuPhos complexes used as catalyst and substrate control in alkylation of bis(secondary phosphines) with benzyl halides, enantioselective tandem alkylation/arylation of primary phosphines

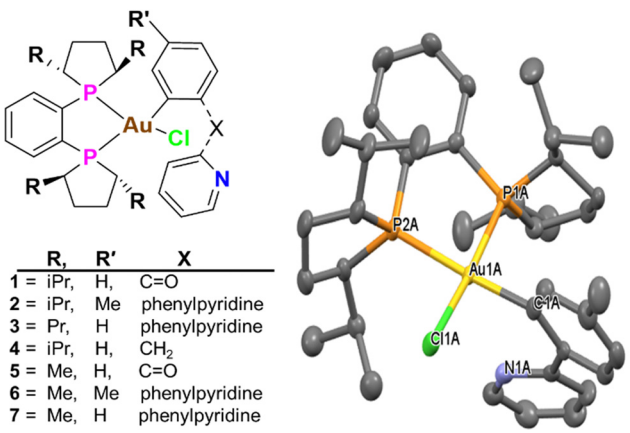

Fig. 1 Chemical structure of complexes **1**–**7** (left) and X-ray crystal structure of **2** with ellipsoids drawn at 50% (right). Hydrogen atoms and solvents have been omitted for clarity.

[a] *Department of Chemistry, University of Kentucky, Lexington, KY 40506, USA. E-mail: awuah@uky.edu*
[b] *Center for Pharmaceutical Research and Innovation and Department of Pharmaceutical Sciences, College of Pharmacy University of Kentucky, Lexington, KY 40536, USA*
[c] *Markey Cancer Center, University of Kentucky, Lexington, KY 40536, USA*

† Electronic supplementary information (ESI) available: Experimental section, Tables S1–S4 and Fig. S1–S59. CCDC 2173747–2173749. For ESI and crystallographic data in CIF or other electronic format see DOI: https://doi.org/10.1039/d2cc03081k

to yield 1-phosphaacenaphthenes.[15] Enantioselective Pd-DuPhos complexes has also been used for homogeneous hydroarylation of norbornene in medium to high enantiomeric excesses,[16] while Rh-DuPhos complexes has been used to catalyze synthesis of α-hydroxy ester with greater than 90% ee.[17]

The novel cationic organometallic Au(III) chlorido complexes [aryl pyridine-Au(III)Cl(R-DuPhos)] (**1–7**; Fig. 1) were synthesized under mild conditions by reacting 2-benzoylpyridine gold(III) dichloride (**1**, **5**), 2-(*p*-tolyl)pyridine gold(III) dichloride (**2**, **6**), 2-phenylpyridine gold(III) dichloride (**3**, **7**), or 2-benzylpyridine gold(III) dichloride (**4**) with 1,2-bis[(2*R*,5*R*)-2,5-dimethyl phospholano]benzene (Me-DuPhos) or 1,2-bis[(2*R*,5*R*)-2,5 diisopropylphospholano]benzene (iPr-Duphos) ligands in dichloromethane at room temperature for 15 minutes. Cyclometallation of conjugated pyridines with transition metals has often been a subject of interest in organic electronics due to the possibility of making highly luminescent materials, yet their use in bioinorganic chemistry is rapidly growing. Also, research into the use of chiral bisphosphine ligands as therapeutic agents are few and underexplored, yet the impact of chirality in drug design cannot be overlooked as the uniqueness of chiral compounds in drug-target affinity can shape a drug's pharmacology. The mild reaction conditions employed in this work, helps to overcome the possibility of reductive elimination reactions associated with donor ligands that react with cyclometallated Au(III) framework.

Complexes **1–7** were characterized by ^{1}H, ^{13}C, and ^{31}P NMR spectroscopy (Fig. S4–S27, ESI†), mass spectrometry (Fig. S32–S38, ESI†), and the purity ascertained by HPLC (Fig. S28–S35, ESI†). It is noteworthy that the ^{31}P NMR of **1–4** (Fig S5, S8, S11 and S14, ESI†) showed 2 additional peaks due to the rotation of isopropyl groups on the 5-membered phospholano ring or a diastereomeric pair. The square planar geometry of [aryl pyridine-Au(III)Cl(R-DuPhos)] was confirmed by X-ray crystallography (Fig. 1 and Fig. S1–S3, Table S1–S3, ESI†) where single crystals were grown by slow diffusion of ether into concentrated acetonitrile or chloroform solution at room temperature for compounds **2** and **3**, or **5**. In the case of **2** and **3**, two complexes per asymmetric unit was found and **2** crystallizes in a monoclinic crystal system while **3** crystallizes in an orthorhombic crystal system with *P*2 space group. Complex **5** crystallizes as a monocationic species with an orthorhombic crystal structure system in a *P*2 space group. Slight distortions to the tune of 3% and 6% of the gold center were observed for the two cationic species in the asymmetric unit of **2**. All complexes showed characteristic bond lengths and bond angles around the Au center reflective of square-planar geometry, including Au–P bond length = 2.28–2.36 Å, Au–Cl bond = 2.34–2.35 Å, while Au–C bond = 2.067–2.076, while the bond angle for C1–Au1–P1 = 92.3–95.5°, C1–Au1–Cl1 = 86.05–89.3° and P1A–Au1A–Cl1A = 173.4–175.4° Also, there was retention of stereochemistry of the complex as seen in the X-ray structures of **2**, **3**, **5** and as predicted by PLATON.[18]

To determine the stability of chiral Au(III) complexes and attendant speciation under physiological conditions, we subjected **1–7** to detailed spectroscopic and liquid chromatography mass spectrometry (LC-MS) investigation. The UV-vis absorption profiles

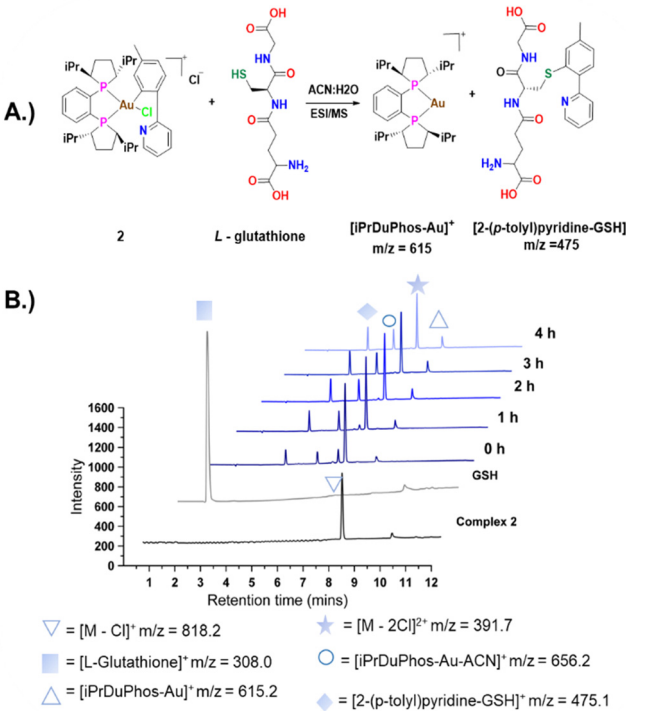

Fig. 2 LC-MS speciation studies with **2** (A) Complex **2** (50 μM in acetonitrile) reacting with L-Glutathione (50 μM in PBS) at room temperature and monitored with LC-MS. (B) Spectra showing adducts formed from studies of **2** with *L*-GSH over 4 h.

of **1–7** (Fig. S43–S49, ESI†) in biologically relevant Dulbecco's modified Eagle's medium (DMEM) revealed minimal alteration over the 18 h period of study at 37 °C for all the complexes studied except **7** which showed reduced stability within 18 h with gold deposit observed which affirms the reduction of **7** (Fig. S49, ESI†). Their absorption spectra showed intense absorption band around 289 nm, characteristic of a metal to ligand charge transfer (MLCT) and the peak at 573 nm can be attributed to ligand centered transitions including interactions of amino acids in DMEM with chiral Au(III) complexes.

Regarding chiral Au(III) speciation, the well-known biological reductant, glutathione (L-GSH), which is present at 10 mM in mammalian cells was incubated with **2** in 1 : 1 ratio and monitored by LC-MS and UV-Vis over a 4 h period (Fig. 2 and Fig. S50–S54, S55, ESI†). We found that upon reaction with GSH, a minor product consistent with reductively eliminated C–S bond compound forms with the prominent parent peak of **2** showing as M^{2+} ion $[M - 2Cl]^{+}$ (m/z = 391.7). Complex **2** is observed throughout the 4 h incubation, however, peaks consistent with reduced Au(I) $[IPrDuPhos\text{-}Au]^{+}$ with m/z = 615.2 or $[IPrDuPhos\text{-}Au\text{-}ACN]^{+}$ adduct with m/z = 656.2 and 2-(*p*-tolyl) pyridine-GSH with m/z = 475.1 increased. To the best of our knowledge this is the first study elucidating chiral Au(III) speciation under reduced biological conditions.

The cytotoxicity of complexes **1–7**, cisplatin, and auranofin were evaluated in four (4) aggressive cancer cells (MDA-MB 468, MDA-MB-231, H460 and BT-333) (Table 1 and Fig. S56–65, ESI†) that lack new therapies. These adherent cells were treated with

the complexes for 72 h at a 3-fold dilution starting from 100 μM. All compounds showed cytotoxicity in the micromolar range with starting ligands dictating their anticancer properties. This is promising as triple negative breast cancer cells are resistant to platinum-based drugs due to multiple cellular pathways. Compounds with the MePhos ligands showed lower cytotoxicity in the nanomolar range in the glioblastoma BT-333 cancer cell line (Table 1). This result is significant in the search for new therapeutics for brain tumor as glioblastoma is one of the most lethal malignant brain tumor types in adults with limited treatment options.[19] Strikingly, the *S*,*S*-isomer of **7** revealed a lower potency across H460, MDA-MB-468, and BT333 cell lines by 2-4-fold in comparison to complex **7**, the *R*,*R*-isomer (Table 1). Chirality may be a differentiating factor in gold drug discovery.

Also, anticancer activity of these complexes in TNBC cell lines (MDA-MB-468 and MDA-MB-231) which are cisplatin-resistant is encouraging for the development of next generation anticancer compounds. Although **7** was potent in the *in vitro* anticancer assays, its reduced stability in DMEM by UV-vis stability studies (Fig S49, ESI†) discouraged its further development. Thus, we prioritized **2** with *p*-tolyl-pyridine and iPrDuPhos ligands due to stability and promising broad spectrum antiproliferative activity for further *in vitro* and *in vivo* studies.

We sought to understand the cell death mechanism of **2** by examining its effect on mitochondria bioenergetics using Seahorse 96 XF instrument (Fig. 3A and B). Simply, we quantified the impact of **2** on oxygen consumption rate (OCR) of cancer cells using known inhibitors of the electron transport chain (ETC). First, **2** was added *via* pneumatic injection which involves high pressured stream of fluid into MDA-MB-231 cancer cell lines. Then, we applied oligomycin (a complex V inhibitor) to quantify the basal OCR, FCCP (a protonophore that helps to uncouple oxidative phosphorylation) enabling the quantification of maximum OCR, and rotenone/antimycin A (a complex I/III inhibitor) to completely shut down the ETC. Results from the seahorse assay (Fig. 3A and B) showed that **2** rapidly and irreversibly inhibited OCR in a dose-dependent fashion. Specifically, 62% decrease in OCR was observed from 1 μM to 10 μM. This suggests that **2** greatly inhibits OCR in MDA-MB-231 to impair cellular energy toward cell death.

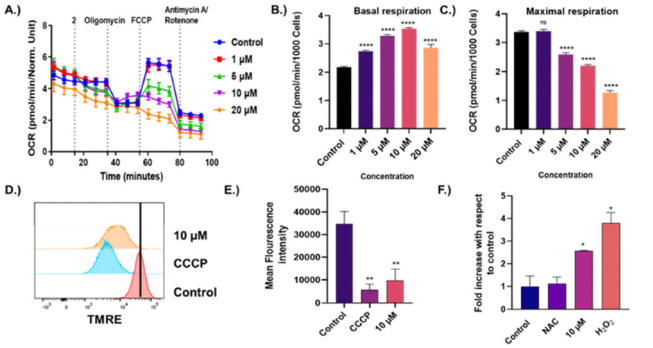

Fig. 3 Evaluation of the mode of cytotoxicity of **2** in TNBC cancer cell lines (A) Mitochondria bioenergetics study using Seahorse assay. Complex **2** was administered *via* pneumatic injection to MDA-MB-231 cancer cells and various inhibitors of ETC was added at various time point. (B and C) Key parameters extrapolated from Seahorse assay. (D and E) MMP determination using TMRE dye. 2 was added at 10 μM for 90 minutes and fluorescence was observed by flow cytometry. (F) ROS determination using DCF-DA dye. **2** was added at 10 μM for 2 h and fluorescence was observed using a fluorescence microscopy with 20X magnification at 488 nm. Ordinary one-way ANOVA, $*P < 0.05$, $**P < 0.01$, $***P < 0.001$, $****P < 0.0001$. ns = not significant.

We further examined the effect of complex **2** on mitochondria membrane potential $\Delta\Psi_m$ (MMP) using a cationic lipophilic dye tetra methyl-rhodamine ethyl ester (TMRE) which readily accumulates in active mitochondria giving rise to red fluorescence that can be detected by flow cytometry. Depolarized mitochondria fail to sequester TMRE and a decrease in membrane potential is observed. After 90 minutes of complex **2** (10 μM) exposure in MDA-MB-468 cells followed by staining with TMRE dye, a decrease in fluorescence intensity was observed for cells treated with complex **2** compared to control cells with no treatment (Fig. 3D and E) suggesting depolarization of the mitochondria membrane potential.

We further accessed the amount of intracellular ROS produced upon addition of complex **2** at 10 μM by using a fluorogenic dye 2′,7′-dichlorofluoresceindiacetate (DCF-DA). 2′,7′-dichlorofluorescein (DCF) produced from deacetylation of DCF-DA is highly fluorescent and can be captured by fluorescence microscopy using the blue light (488 nm) excitation filter. MDA-MB-468 cells were treated with 10 μM of complex **2** for 2 h, hydrogen peroxide was used as positive control while 20 mM of *N*-acetyl cysteine (NAC) was added to pre-treatment wells for 2 h prior to the addition of **2**. NAC is a scavenger of peroxides, and it helps to differentiate fluorescence from ROS from other species such as RNS. Fig. 3F and Fig. S67, ESI† shows that there was more than 2-fold increase in the florescent intensity of 2 at 10 μM compared to the control. This result indicates that 2 induces ROS production and this could be a major contributor to cell cytotoxicity.

Au(III) complexes are known to induce apoptosis in cancer cells, we therefore evaluated the ability of **2** to induce apoptosis

Table 1 Table showing IC_{50} values for complex **1–7**, cisplatin and auranofin in MDA-MB-468, MDA-MB-231, H460 and BT-333 cancer cell lines

Compounds	MDA-MB-468	MDA-MB-231	H460	BT333
1	1.74 ± 0.36	1.1 ± 0.15	0.48 ± 0.20	4.43 ± 0.07
2	1.3 ± 0.35	1.44 ± 0.15	2.75 ± 0.16	2.95 ± 0.04
3	5.01 ± 0.35	4.33 ± 0.14	11.48 ± 0.16	4.57 ± 0.069
4	1.07 ± 0.36	1.28 ± 0.16	0.59 ± 0.15	2.14 ± 0.09
5	1.62 ± 0.06	2.19 ± 0.06	2.29 ± 0.06	0.219 ± 0.02
6	3.16 ± 0.07	1.51 ± 0.1	5.75 ± 0.1	0.62 ± 0.014
7	1.18 ± 0.05	0.46 ± 0.06	1.0 ± 0.007	0.095 ± 0.12
S,*S*-Isomer of 7	3.8 ± 0.05	0.69 ± 0.02	3.8 ± 0.03	0.23 ± 0.01
Cisplatin	4.16 ± 0.02	34.56 ± 0.783[a]	5.63 ± 1.02[a]	>100
Auranofin	1.58 ± 0.03	0.616 ± 0.01	1.2 ± 0.03	4.8 ± 0.01

[a] Reported IC_{50} values of cisplatin in MDA-MB-231 and H460 respectively.[6,20]

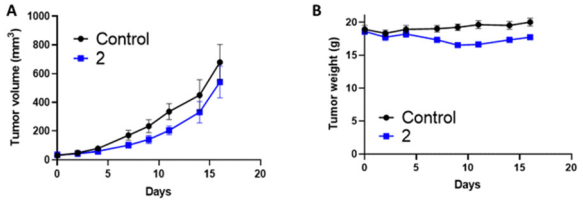

Fig. 4 Complex **2** inhibited 4T1 in Balb/c mice (A) Tumor volume of murine 4T1 model in Balb/c mice show overall decrease in tumor volume compared to control with 14 days (B) Body weight of murine 4T1 in Balb/c mice. No significant difference was observed in the body weight after 14 days of treatment.

in MDA-MB-468 at 24 h. Using the fluorescence-assisted cell-sorting (FACS) analysis, we examined the number of cells undergoing apoptosis by adding Annexin V a protein that binds phosphatidylserine (PS) abundant in cells undergoing apoptosis. A fluorescent tag (FITC) is labelled with Annexin V to ensure visualization in the green channel of FACS. Propidium iodide is then added to distinguish between the DNA of cells undergoing necrosis from those undergoing apoptotic cell death. MDA-MB-468 cells were treated with **2** at 1.3 μM and 2.5 μM for 24 h, Fig S66, ESI† shows that **2** induces a low apoptotic population within 24 h. It is important to note that metallodrugs induce cell death *via* several mechanisms such as ferroptosis, necrosis, and apoptosis. These other modes of cell death will be the subject of study in future work.

To determine the efficacy of **2** *in vivo*, Balb/c mice inoculated with 4T1 cancer cells were treated with **2** at a concentration of 10 mg kg^{-1} every other day 3 times per week. The treatment group was compared to a control group that was treated with a PBS solution containing 1% DMSO and 10% Kolliphor (vehicle). The tumor volume and the body weight of the treated and control mice was recorded every other day. Within the first 3 days of tumor cell implantation, all mice showed equal tumor volume before a gradual increase in tumor volume after 3 days (Fig. 4). After the treatment period of 14 days, all mice were recorded with no significant difference in body weight and a modest decrease in tumor volume, which was not statistically significant in a student *t*-test analysis. Although promising, optimization of the treatment regimen or structure will be needed. This result suggests that **2** is tolerable in mice and it is a good candidate for anticancer drug development.

In conclusion, this study has identified promising chiral Au(III) anticancer agents [2-arylpyridine-Au(III)Cl(alkyl-DuPhos)] complexes. The ease of preparation of these complexes was followed by purification with chromatographic techniques and spectroscopic characterization by NMR, ESI-MS and UV-vis. The bioanalysis of [2-*p*-(tolyl)pyridine-Au(III)Cl(iPr-DuPhos)] **2** showed improved potency compared to the FDA approved anticancer metallodrug cisplatin in TNBC resistant cell MDA-MB-231 and glioblastoma cancer cell BT-333. The speciation studies also enabled for the first time elucidation of the products from a chiral Au(III) complex, **2** with L-glutathione. Also, **2** inhibited oxygen consumption rate in TNBC in the mitostress assay and showed depolarization of the mitochondria membrane potential with intracellular ROS production pointing towards its mode of cytotoxic action. These results showed that chiral Au(III) complexes can play a role in development of next generation anticancer agents.

We are grateful for financial support from the National Cancer Institute (NCI) R01CA258421-01 (S. G. A.). We would like to thank all the facilities at the University of Kentucky who provided support in completion of the experiments detailed in this manuscript. The UK NMR Center supported by NSF (CHE-997738) and the UK X-ray facility supported by the MRI program from NSF (CHE-1625732). For the flow cytometry experiments we would like to thank UK Flow Cytometry and Immune Function core supported by the Office of the Vice President of Research, the Markey Cancer Center, and NCI Center Core Support Grant (P30 CA177558). We thank Dr Chris Richard's lab for access and assistance with fluorescence microscopy. We would also like to thank Tomoko Sengoku PhD and Mr Michael Alstott for the support with our redox metabolism experiments, supported by the shared resource(s) of the University of Kentucky Markey Cancer Center (P30CA177558).

Conflicts of interest

There are no conflicts to declare.

References

1 C. F. Shaw, *Chem. Rev.*, 1999, **99**, 2589–2600.
2 C. X. Zhang and S. J. Lippard, *Curr. Opin. Chem. Biol.*, 2003, **7**, 481–489.
3 K. D. Mjos and C. Orvig, *Chem. Rev.*, 2014, **114**, 4540–4563.
4 T. Zou, C. T. Lum, C.-N. Lok, J.-J. Zhang and C.-M. Che, *Chem. Soc. Rev.*, 2015, **44**, 8786–8801.
5 S. Gukathasan and S. G. Awuah, *Encycl. Inorg. Bioinorg. Chem.*, 2022, 1–32.
6 J. H. Kim, E. Reeder, S. Parkin and S. G. Awuah, *Sci. Rep.*, 2019, **9**, 1–18.
7 R. Jouhannet, S. Dagorne, A. Blanc and P. de Frémont, *Chem. – Eur. J.*, 2021, **27**, 9218–9240.
8 P. T. Bohan and F. D. Toste, *J. Am. Chem. Soc.*, 2017, **139**, 11016–11019.
9 J. J. Jiang and M. K. Wong, *Chem. – Asian J.*, 2021, **16**, 364–377.
10 C. Olelewe, J. H. Kim, S. Ofori, R. T. Mertens, S. Gukathasan and S. G. Awuah, *iScience*, 2022, 104340.
11 D. Gasperini, M. D. Greenhalgh, R. Imad, S. Siddiqui, A. Malik, F. Arshad, M. I. Choudhary, A. M. Al-Majid, D. B. Cordes and A. M. Slawin, *Chem. – Eur. J.*, 2019, **25**, 1064–1075.
12 S. Gukathasan, S. Parkin and S. G. Awuah, *Inorg. Chem.*, 2019, **58**, 9326–9340.
13 A. S. Arojojoye, R. T. Mertens, S. Ofori, S. R. Parkin and S. G. Awuah, *Molecules*, 2020, **25**, 5735.
14 J. H. Kim, S. Ofori, S. Parkin, H. Vekaria, P. G. Sullivan and S. G. Awuah, *Chem. Sci.*, 2021, **12**, 7467–7479.
15 B. J. Anderson, M. A. Guino-o, D. S. Glueck, J. A. Golen, A. G. DiPasquale, L. M. Liable-Sands and A. L. Rheingold, *Org. Lett.*, 2008, **10**, 4425–4428.
16 D. Drago and P. S. Pregosin, *Organometallics*, 2002, **21**, 1208–1215.
17 M. J. Burk, C. S. Kalberg and A. Pizzano, *J. Am. Chem. Soc.*, 1998, **120**, 4345–4353.
18 A. L. Spek, *Acta Crystallogr., Sect. D: Biol. Crystallogr.*, 2009, **65**, 148–155.
19 Q. T. Ostrom, G. Cioffi, H. Gittleman, N. Patil, K. Waite, C. Kruchko and J. S. Barnholtz-Sloan, *Neuro-Oncology*, 2019, **21**, v1–v100.
20 R. T. Mertens, W. C. Jennings, S. Ofori, J. H. Kim, S. Parkin, G. F. Kwakye and S. G. Awuah, *JACS Au*, 2021, **1**, 439–449.

